Journal of Applied Physics

RESEARCH ARTICLE | MARCH 04 2024

Room temperature electrical characteristics of gold-hyperdoped silicon

Shao Qi Lim ; Jeffrey M. Warrender ; Christian Notthoff ; Thomas Ratcliff ; Jim S. Williams ;
Brett C. Johnson

J. Appl. Phys. 135, 095704 (2024)
https://doi.org/10.1063/5.0196985

04 September 2024 02:21:17

Journal of Applied Physics ARTICLE pubs.aip.org/aip/jap

Room temperature electrical characteristics of gold-hyperdoped silicon

Cite as: J. Appl. Phys. 135, 095704 (2024); doi: 10.1063/5.0196985
Submitted: 10 January 2024 · Accepted: 16 February 2024 ·
Published Online: 4 March 2024

View Online

Export Citation

CrossMark

Shao Qi Lim,[1,2,a)] Jeffrey M. Warrender,[3] Christian Notthoff,[1] Thomas Ratcliff,[1] Jim S. Williams,[1] and Brett C. Johnson[4]

AFFILIATIONS

[1]Research School of Physics, The Australian National University, Canberra 2601, ACT, Australia
[2]CQC^{2}T, School of Physics, University of Melbourne, Parkville 3010, VIC, Australia
[3]U.S. Army Combat Capabilities Development Command—Armaments Center, Watervliet, New York 12189, USA
[4]School of Science, RMIT University, Melbourne, VIC, 3001, Australia

[a)]**Author to whom correspondence should be addressed:** qi.lim@unimelb.edu.au

ABSTRACT

Hyperdoped silicon is a promising material for near-infrared light detection, but to date, the device efficiency has been limited. To optimize photodetectors based on this material that operate at room temperature, we present a detailed study on the electrical nature of gold-hyperdoped silicon formed via ion implantation and pulsed-laser melting (PLM). After PLM processing, oxygen-rich and gold-rich surface layers were identified and a wet etch process was developed to remove them. Resistivity and Hall effect measurements were performed at various stages of device processing. The underlying gold-hyperdoped silicon was found to be semi-insulating, regardless of whether the surface gold was removed by etching or not. We propose a Fermi level pinning model to describe the band bending of the transformed surface layer and propose a promising device architecture for efficient Au-hyperdoped Si photodetectors.

© 2024 Author(s). All article content, except where otherwise noted, is licensed under a Creative Commons Attribution (CC BY) license (http://creativecommons.org/licenses/by/4.0/). https://doi.org/10.1063/5.0196985

04 September 2024 02:21:17

I. INTRODUCTION

Hyperdoped semiconductors contain an intermediate band (IB, a.k.a. impurity band) within the bandgap that can be employed to efficiently absorb light with below bandgap energies and are promising candidates for Si-based near-infrared (NIR) photodetectors.[1–3] These materials are typically fabricated by ion implantation of a suitable impurity followed by pulsed laser melting (PLM) to achieve the high impurity concentrations required to form an IB (6×10^{19} cm^{-3} for Si[4]).

Among the various transition metal impurities explored to date, gold (Au) is the only impurity that can be homogeneously hyperdoped in mono-crystalline Si up to concentrations of 10^{20} cm^{-3}, above which filamentary breakdown takes place.[5,6] Other impurities tend to segregate completely or exhibit filamentary breakdown.[7,8] Despite showing broadband NIR optical absorption and photoresponse, Au-hyperdoped Si detectors have an extremely low quantum efficiency ($< 0.01\%$),[6] which has been attributed to poor carrier transport and carrier lifetime properties within the hyperdoped layer (10–800 ps).[9–12] We have recently suggested that the NIR light detection efficiency in Au-hyperdoped Si devices at room temperature (RT) can be improved with an optimized device architecture.[10] To achieve this, accurate knowledge of the surface properties and RT electrical characteristics of the Au-hyperdoped layer is required.

In terms of the surface properties, it is well known that some degree of Au surface segregation will occur during the PLM process due to the high interface diffusivity of Au and the low solid solubility of Au in the solid phase of Si as compared to its liquid phase.[1,2,13] This phenomenon is well evidenced by Rutherford backscattering spectrometry and ion channeling (RBS-C) and secondary ion mass spectrometry measurements.[6,7,9,11,14] It is also expected that the Si surface may become oxidized during the PLM process. This will greatly impact the quality of metallic contacts formed directly on the Au-hyperdoped Si. In turn, this can complicate interpretation of near-surface electrical measurements.

As for the electrical properties of Au-hyperdoped Si, a number of reports have suggested that Au-hyperdoped Si is p-type

© Author(s) 2024

at RT, displaying hole conduction characteristics.[6,9,10,15] The earliest report was by Weman *et al.*[15] based on Hall effect measurements of Au in-diffused n-type Si. More recently, rectifying current–voltage (I–V) characteristics were reported on Au-hyperdoped Si fabricated on a n-type Si substrate, while Ohmic behavior was observed when it was fabricated on a p-type substrate.[6] The origin of this type conversion remains poorly understood[16] and appears to be in contradiction with the established theoretical understanding of IB semiconductors.[17–19] In the context of Au-hyperdoped Si, it is well known that Au introduces two deep levels in the Si bandgap ($\gg 3k_BT$), located at $E_{Au,d} - E_v = 0.35$ eV and $E_c - E_{Au,a} = 0.53$ eV, respectively [where $E_{v,c}$ are the Si valence/conduction band (VB/CB) edges].[19] These deep lying Au states are not expected to ionize at RT and contribute to conduction. Rather, a Au-IB is expected to form near midgap and the Au-hyperdoped layer's Fermi level is expected to be located within the IB.[19]

Here, we investigate the impact of the surface on the measured electrical characteristics of Au-hyperdoped Si formed by ion implantation and PLM. We first focus on the physical surface properties of Au-hyperdoped Si. Wet etching experiments are combined with RBS-C measurements to gain a better understanding of the Au-hyperdoped Si surface. Van der Pauw resistivity and Hall measurements are then reported. Finally, we discuss the origin of the so-called anomalous n-to-p type-conversion phenomenon described above.

II. EXPERIMENTAL METHOD

Au-hyperdoped Si samples were fabricated by ion implantation and PLM as described in our previous works.[6,9,10] Briefly, Au^+ ions at 300 keV were implanted into a semi-insulating float-zone Si substrate (sourced from Topsil Global Wafers, $\rho > 10\,k\Omega$ cm, ⟨100⟩, 310–340 μm thick) held at 77 K at an ion fluence of 10^{15} cm^{-2}. The high resistivity ensures that a doped surface remains electrically isolated from the substrate. Indeed, this behavior has been confirmed with implanted Bi on similar substrates.[20] During implantation, the Si substrate was tilted by 15° and rotated by 7° to minimize ion channeling. PLM was then performed with a single 6 ns pulse of the third harmonic (355 nm) of a Nd:YAG laser (Ekspla) over a 2.5×2.5 mm^2 aperture to a nominal fluence of 0.85 ± 0.05 J/cm^2. A schematic of the PLM process and sample cross section after PLM together with the resultant Au concentration profile is shown in Fig. 1. The melt duration was monitored using time-resolved reflectivity with a 488 nm Ar^+ ion laser. The PLM was tiled in a 2×2 configuration with a slight overlap to create a single Au-hyperdoped Si sample with an area just under 5×5 mm^2. The sample was then diced along the perimeter of the PLM region into a 4×4 mm^2 chip with an Oxford Lasers ALPHA 532-XYZ-A-A Laser Micromachining Tool to electrically isolate it from the surrounding amorphous Au-implanted region. All samples were then subjected to sonication in acetone, IPA, and DI-H_2O, followed by various wet etch procedures described in Sec. III A.

The surface chemical composition of the Au-hyperdoped Si sample was characterized with Rutherford backscattering spectrometry with ion channeling (RBS-C). A 1 MeV He^+ ion beam was directed onto the sample surface and the backscattered ions were

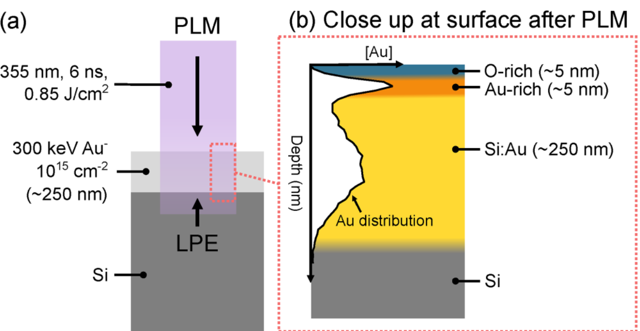

FIG. 1. (a) Schematic of the PLM process. Rapid solidification and liquid phase epitaxy (LPE) occurs within hundreds of nanoseconds following the laser pulse. (b) Sample cross section after PLM, showing the O-rich layer at the surface (blue), the Au-rich layer (orange) underneath due to Au surface segregation from PLM, and the underlying Au-hyperdoped layer (yellow). The Au concentration [Au] distribution is shown as a black trace shaded white (data are the same as that shown in Fig. 2 labeled "as-PLM").

detected with a solid state detector placed at an angle of $\theta = 170°$. The detector resolution is around 15 keV.

RT electrical resistivity and Hall effect measurements were performed on companion samples (without any RBS-induced damage) after various wet etching processes (described in Secs. III A and III B). For contact formation, sample electrodes were placed at the corners of the device in a van der Pauw configuration. The electrodes were formed with electron beam evaporation of Al through a shadow mask. All measurements were performed at RT under dark conditions. The four-terminal I–V measurements were made between $\pm 1.0\,\mu$A with each possible contact combination to account for any device asymmetries. All devices exhibited linear I–V curves with a R-squared correlation value between 0.998 and 1.0, indicating that the contacts are Ohmic in nature. The two-terminal resistance extracted from the slopes of these I–V curves, R_{ij}, ranged between 1.73 and 2.83 MΩ.

The Hall measurements was conducted with B-field sweeps between ± 1.0 T, in steps of 0.1 T. The Hall parameters, $R_{H,s}$ (sheet Hall coefficient), n_s (sheet carrier concentration), and μ_s (sheet mobility), at a particular B-field magnitude are then calculated by averaging over the positive and negative field values.

III. RESULTS AND DISCUSSION

A. Surface etching experiments

To electrically contact the Au-hyperdoped Si effectively, a series of wet chemical processes were investigated. Figure 2(a) schematically shows the samples after each processing step. A Si substrate with a native surface oxide [Fig. 2(a)(i)] was implanted with Au and PLM processed [Fig. 2(a)(ii)] as described above. Afterward the sample was cleaned in Piranha (10 min in H_2SO_4:H_2O_2 = 4 : 1 at 90°C), dilute HF (5%, 10 s), and RCA2 (10 min in HCl:H_2O_2:H_2O = 1:1:5 at 90°C). A longer HF etch was performed for 60 s [Fig. 2(a)(iii)]. This was followed by a Au etch process, which involves repeatedly etching (three times) in HF for 45–60 s

04 September 2024 02:21:17

© Author(s) 2024

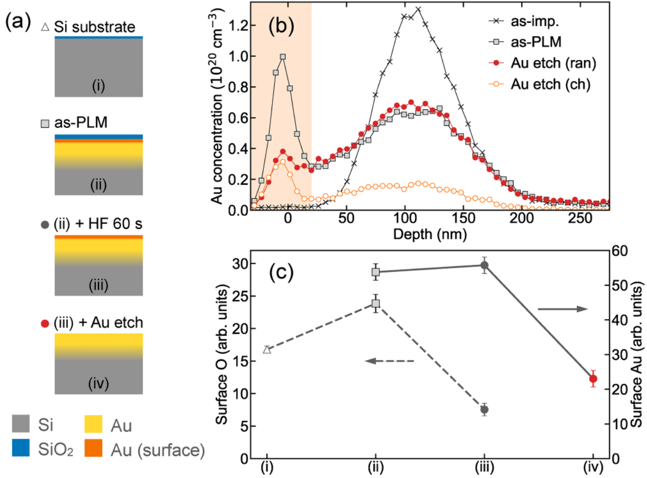

FIG. 2. (a) Schematic cross sections of samples after various processing steps: (i) Si substrate with native oxide (pristine); (ii) after Au ion implantation and PLM, i.e., "as-PLM" Au-hyperdoped Si [same as Fig. 1(b)]; (iii) Au-hyperdoped Si sample in (ii) after 60 s etch in dilute HF; (iv) sample (iii) after Au etch. (b) Au concentration profiles of as-implanted, as-PLM, and Au-etched samples, calculated from their respective RBS spectra with the RUMP RBS simulation and analysis software package.[21] The difference between the RBS random (ran) and channeled (ch) spectra represents the fraction of substitutional Au in the Si lattice. (c) Integrated RBS yield of the surface O and Au signals (normalized by the total collected charge) after different stages of sample processing depicted in (a). These O and Au integrated yields are directly proportional to the O and Au concentration at the surface, respectively. The integration region used to measure the surface Au yield is highlighted in orange in (b).

followed by an 8 min aqua regia etch (3:1 of HCl and HNO_3) [Fig. 2(a)(iv)].

The surface Au depth profile determined from RBS is presented in Fig. 2(b). The as-implanted Gaussian-like profile has a projected range of 110 nm. PLM causes a large concentration of Au to segregate at the surface while the bulk Au concentration reduces by a factor of two. After HF and Au etches [Fig. 2(a)(iv)], the Au surface peak decreases to a concentration that is below the maximum concentration in the bulk (4 and 7×10^{19} cm^{-3}, respectively). Importantly, the surface Au is observed to be partially substitutional after Au etching ($38 \pm 2\%$) as indicated by the difference in the random and channeled RBS spectra [solid red and hollow yellow data in Fig. 2(b), respectively], noting that in RBS-C, a random measurement detects the total Au in the substrate while a channeled measurement detects the non-substitutional component of the Au. There are several possible reasons that may contribute to the apparent substitutionality of surface Au: (1) limited depth resolution of our RBS-C instrument makes it difficult to resolve Au that is between the surface oxide and underlying Si from Au that is incorporated within the first few nm of the underlying Si, which may be partially substitutional; (2) a small amount of surface Au that is not in the Si lattice may have agglomerated laterally and these agglomerates (small precipitates) may be partially aligned with the underlying Si crystal; (3) some of the Au atoms may have formed small zones of Au–Si eutectic alloy at the surface which may also exhibit some alignment with surrounding and underlying Si.[5] Substitutional Au is a key requirement for optical and electrical activation of Au in the hyperdoped layer.[2,3] It is, therefore, critical to develop methods to remove the surface Au layer, which will enable direct access to the Au-hyperdoped layer in the bulk component of the profile where the Au substitutional fraction is substantially higher ($79.8 \pm 0.4\%$). We further note that a triangulation procedure along three crystallographic axes is typically required in RBS-C to determine substitutionality unequivocally, and that the channeled measurement shown in Fig. 2(b) was performed along the $\langle 100 \rangle$ direction only. Thus, the Au substitutional fractions reported in our work serve only as a first approximation.

Figure 2(c) shows the integrated O and Au concentrations at the Si surface determined by RBS. It is observed that the PLM process results in an increase in the surface oxide thickness [denoted as a blue layer in Fig. 2(a)(ii)]. This is consistent with our previous reports in Ag-hyperdoped Si.[8] Other than the high temperatures experienced by the Si during PLM in atmosphere, oxidation may also result from Au and Ag acting as oxidation catalysts in Si.[22,23] A HF etch of 60 s is shown to remove this oxide. We find that at least 45 s of HF etching is required for its removal and greater than 60 s did not appear to reduce the O content any further. The small persisting O signal is presumably due to near surface O beneath the surface and/or oxide regrowth during sample transport between the HF lab and the RBS sample chamber.

As observed in Fig. 2(b), a large concentration of Au also segregates to the surface during PLM [orange layer in Figs. 2(a)(iii) and 2(b)]. The depth resolution of the RBS detector is not high enough to determine the exact composition of these surface layers and whether they are intermixed. However, we find that, although the 60 s HF etch is sufficient to remove the surface oxide, there is no corresponding change in the Au concentration [Fig. 2(c) step (ii) to (iii)]. This suggests that the Au is not necessarily embedded in the oxide layer, but rather located underneath the surface oxide, possibly near the Si/SiO_2 interface.

A Au etch process was then performed after the 60 s HF using an 8 min aqua regia etch, which is strongly oxidizing. This HF-aqua regia etch sequence was repeated three times. The Au surface concentration was observed to gradually decrease after each successive step. The final surface profile after three etch repetitions was found to reduce by a factor of over two, as shown in Figs. 2(b) and 2(c).

Importantly, we find that a similar reduction in the surface Au concentration is not possible with either HF or aqua regia alone, at least for up to a 30 min etch duration as confirmed with RBS measurements (not shown). Specifically, samples were etched in aqua regia for durations ranging from 2 to 30 min. After about 8 min of etching in aqua regia, the surface Au peak did not decrease further. Simultaneously, the surface oxygen peak increased with increasing etch duration up to the 8 min mark as a result of the strongly oxidizing HNO_3 (this oxidation may also be enhanced by the presence of the Au which may act as a catalyst for oxidation of Si[22,23]). This further suggests that the segregated surface Au exists within the Si rather than the surface oxide. Thus, etching the surface Au is limited by the re-oxidation of the surface during the aqua regia process after 8 min. Alternating an aqua regia etch with relatively

04 September 2024 02:21:17

© Author(s) 2024

long HF etching is therefore key to removing the surface Au. This process allows fine control over the etching of the surface, enabling direct electrical connection to the underlying Au-hyperdoped Si layer. Finally, we note that our previous reactive ion etching experiments[11] were less successful at removing the surface segregated gold than the wet etching process presented here, for reasons that remain elusive.

B. Electrical measurements

Three van der Pauw samples were prepared for resistivity and Hall effect measurements, including an intrinsic Si sample [substrate control, Fig. 2(a)(i)], Au-hyperdoped Si sample after 60 s etching in dilute HF [HF 60 s, Fig. 2(a)(iii)], and Au-hyperdoped Si sample after the Au etch procedure [Au etch, Fig. 2(a)(iv)]. Before the evaporation of the Al electrodes, these samples were further etched in dilute HF to remove the surface oxide (otherwise, the I–V characteristics of our devices become non-linear). In short, after device processing, the surfaces of our three devices consist of either a clean Si surface, Au-hyperdoped Si with a significant Au segregated surface, or Au-hyperdoped Si with a greatly reduced Au segregated surface.

The resistivity and Hall results are summarized in Table I. The sheet values (cm^{-2}) are shown instead of the bulk values (cm^{-3}) since the thicknesses of the conductive layers are not well defined. We note that, for the substrate control sample, at a field of 1 T, the bulk resistivity is $\rho = R_s \times t = 37\,k\Omega\,cm$, and the bulk carrier concentration is $n = n_s \times t = 1.33 \times 10^{11}\,cm^{-3}$, where $t = 325\,\mu m$, in good agreement with the supplier's specifications.

We now focus on the sign of the Hall coefficients ($R_{H,s}$) shown in Table I. For the substrate control sample, it is measured to be negative, indicating that the free majority carriers are electrons. Interestingly, $R_{H,s}$ is also negative in our Au-hyperdoped Si samples (both after HF 60 s and Au etch). One possible explanation is that Au is acting as an ionizing donor. However, we do not expect the Au deep donor level, ($E_{Au,d} - E_v = 0.35\,eV$) to be ionized under the experimental conditions applied (RT and dark conditions). Another more plausible explanation is that we are measuring the substrate. This is supported by similar van de Pauw Hall measurements that we performed on Au-hyperdoped Si samples fabricated on conductive n and p-type Si substrates ($\rho = 1-10\,\Omega.cm$) (not shown). In both cases, the sign of $R_{H,s}$ was observed to depend on the substrate (positive for the p-type substrate and negative for the n-type substrate). In the context of the Au-hyperdoped Si samples in Table I, measurement of the substrate implies that the Au-hyperdoped Si layer is, like the substrate, also semi-insulating, irrespective of whether the surface segregated Au is etched away or not. We note that, if Au-hyperdoped Si is indeed semi-insulating, it would also imply that electrical isolation from the substrate may not be completely achieved, and, therefore, the values in Table I may not accurately reflect the exact values for Au-hyperdoped Si. This lack of electrical isolation between the hyperdoped layer and the substrate is a known issue and has been reported in Ti-hyperdoped Si.[24] Nevertheless, the carrier mobility of the substrate clearly decreases after Au-hyperdoping despite the 50% increase in n_s. These trends are consistent with observations on Ti-hyperdoped Si[24,25] and were previously associated with the formation of an IB.[24,26] Another possibility is that the Au atoms (and a range of additional defects introduced during sample fabrication) are acting as efficient scattering and generation–recombination centers.[9–11,27]

TABLE I. RT sheet resistance and Hall parameters (at $|B| = 1$ T) for substrate control, Au-hyperdoped Si after 60 s HF [Fig. 2(a)(iii)] and Au-etched [Fig. 2(a)(iv)] samples. A percentage error of 5% is assumed due to sample geometry correction factors.

Parameter	Substrate control	HF 60 s	Au etch
R_s (kΩ)	1130	870	829
$R_{H,s}$ ($\times 10^8\,cm^2/C$)	−14.4	−9.58	−9.45
n_s ($\times 10^9\,cm^{-2}$)	4.33	6.51	6.61
μ_s ($cm^2/(V\,s)$)	1300	1130	1160

C. Fermi level pinning model

We propose a surface Fermi level pinning model and discuss how it may adequately explain the aforementioned n-to-p-type conversion phenomena in Au-hyperdoped Si at *RT*. The surface band diagram of our Fermi level pinning model is shown in Fig. 3(a). From theory,[19] the Au-hyperdoped layer, which has a peak Au concentration in the bulk of $7 \times 10^{19}\,cm^{-3}$ in our work [Fig. 2(b)], should result in the formation of a partially filled IB in the Si bandgap located between the two Au deep donor and acceptor energy levels. At RT and under the dark measurement conditions employed, we do not expect the IB to be ionized and thus, the Fermi level will appear within the IB. Note that even though this Fermi level model agrees well with our observation that Au-hyperdoped Si is semi-insulating, we acknowledge that this

04 September 2024 02:21:17

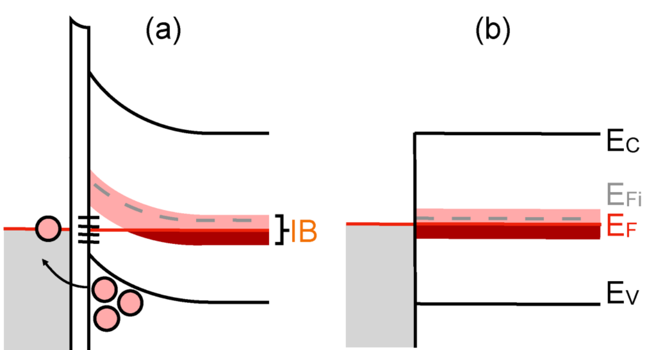

FIG. 3. Proposed band diagram under equilibrium conditions (zero bias) of (a) Au-hyperdoped Si with an interface layer of atomic dimensions (a few Å, either from a mildly oxidized surface or a vacuum layer[28]) and segregated Au sandwiched between it and the metal contact (Al); (b) Au-hyperdoped Si directly in contact with metal, assuming perfectly ideal conditions with no surface states or band bending. Pink dots represent hole carriers, gray area represents electrons in the Al metal, pink (dark red) area represents empty (filled) states in the Au-IB, acceptor states due to interaction between Au and surface/interface states are represented by black solid lines. The red solid line represents the Fermi level (E_F) while the intrinsic Fermi level in Si (E_{Fi}) is represented by dashed gray lines. The VB/CB edge is indicated by E_V/E_C.

© Author(s) 2024

observation alone does not constitute evidence for the formation of a partially filled Au-IB nor the location of the Fermi level, as will be discussed later.

It is well known that surface states can pin the Si Fermi level at the surface even before contact metalization.[28] Furthermore, it has been previously shown that the segregated Au at the Si/SiO_2 interface interacts with surface/interfacial disorder defects to produce acceptor states at this interface that are within 0.16 eV from the VB edge,[29] noting that these states are not the same as the *bulk* acceptor state of Au located at $E_c - E_{Au,a} = 0.53$ eV. We believe that Au-related *surface* acceptor states close to the VB edge are also present in our Au-hyperdoped Si samples at high densities. These surface acceptor states are expected in all of our Au-hyperdoped Si samples before and after the various wet etching processes described above [i.e., samples depicted in Fig. 2(a)(ii–iv)] and vary in terms of the acceptor state energy level in the bandgap and density. The former depends on the specific physical and chemical nature of the surface, while the latter depends on thesurface/interfacial disorder defect and Au densities at the surface/interface. Due to high density of Au from hyperdoping, these Au-related surface acceptor states can result in the Fermi level being pinned to near the VB edge *at the surface* and subsequent band bending. This effect is illustrated in Fig. 3(a), where the Fermi level is assumed to be pinned in the middle of a distribution of Au-related surface acceptor states. We note that Fig. 3(a) is not a simulation; it is a simplified sketch of the surface band bending in our samples to help illustrate our model, and does not account for other physical effects such as charges due to occupancy of acceptor states and subsequently induced charges at the metal surface and Si space charge region.[28] A sketch of the band diagram in the ideal case in absence of surface states and with intimate contacting between the Au-hyperdoped Si and Al metal is also shown in Fig. 3(b). Here, the Fermi level is instead pinned to within the Au-IB near the intrinsic level, as established from theory.[17–19] However, due to the presence of high concentrations of Au from hyperdoping, we do not believe that it is possible to eliminate the aforementioned Au-related surface acceptor states and unpin the Fermi level *at the surface*, even after removing the surface segregated Au.

From Fig. 3(a), it is clear that Fermi level pinning causes the surface bands to bend in the same way as if the surface was heavily doped with shallow p-type dopants. This enables the formation of Ohmic contacts to the semi-insulating Au-hyperdoped Si, as suggested by our Hall effect measurements.[30] Furthermore, under our Fermi level pinning model, it is expected that Au-hyperdoped Si will be rectifying on n-type Si substrates and Ohmic on p-type substrates, as observed in the literature.[6,9,10] In light of recent reports on Ti-hyperdoped Si in the literature,[25] it may be beneficial to perform further measurements on Au-hyperdoped Si at low temperatures to achieve electrical isolation from the substrate and to confirm the formation of a Au-IB. Additionally, x-ray techniques may also be employed to elucidate the location of the Fermi level and provide further evidence that supports the existing theory.[19]

Finally, in the context of fabricating Au-hyperdoped Si optoelectronic devices that operate at RT,[6,31] our results suggest that it may be more fruitful to pursue a *lateral* device architecture where Au-hyperdoped Si is fabricated on semi-insulating Si substrates with separate p and n-type layers, much like a lateral pin junction diode. Electron and hole selective Ohmic contacts can then be made separately to the n and p-type regions, respectively, as suggested also by Ref. 18. Furthermore, considering the low carrier lifetime and mobility in the Au-hyperdoped Si layer,[11,26] it may also be beneficial to implement a lateral pin structure with a closely spaced, interdigitated pattern to reduce the carrier diffusion length and thus improve photo-detection efficiency.

IV. CONCLUSION

To summarize, the extensive use of the RBS-C technique has provided us with a better understanding of the surface properties of Au-hyperdoped Si and has enabled us to develop a reliable wet etching protocol that removes the enhanced surface oxide and reduces the amount of surface segregated Au. This allowed us to gain a better understanding of the electrical characteristics of the Au-hyperdoped Si at RT and investigate the effect of the Au surface segregation. Hall effect measurements indicate that our Au-hyperdoped Si samples are semi-insulating at RT, in agreement with theoretical predictions. Furthermore, previous experimental observations of p-type conduction in Au-hyperdoped Si may be a result of Fermi level pinning at the surface and subsequent band bending, and/or measurement of the substrate. Additional X-ray measurements and low temperature photoconductivity measurements may provide a more robust confirmation of theoretical predictions about the formation of a Au-IB in our samples, the location of the Fermi level, and whether Au-hyperdoped silicon will lead to useful applications in optoelectronics. Our work provides insight into the surface properties of Au-hyperdoped Si and proposes a method to fabricate Au-hyperdoped Si photodetectors that operate at RT with improved reliability and efficiency.

04 September 2024 02:21:17

ACKNOWLEDGMENTS

This work is supported by the U.S. Army (Contract No. FA5209-16-P-0104). We acknowledge access and support to NCRIS facilities (ANFF and the Heavy Ion Accelerator Capability) at the Australian National University and the University of Melbourne.

AUTHOR DECLARATIONS

Conflict of Interest

The authors have no conflicts to disclose.

Author Contributions

Shao Qi Lim: Conceptualization (lead); Data curation (lead); Formal analysis (lead); Investigation (lead); Methodology (lead); Writing – original draft (lead); Writing – review & editing (lead). **Jeffrey M. Warrender:** Funding acquisition (equal); Methodology (equal); Resources (equal); Validation (equal); Writing – review & editing (equal). **Christian Notthoff:** Investigation (equal); Methodology (equal); Validation (equal). **Thomas Ratcliff:** Methodology (equal); Resources (equal). **Jim S. Williams:** Conceptualization (equal); Formal analysis (equal); Funding acquisition (equal); Investigation (equal); Project administration (equal); Resources (equal); Supervision (lead); Validation (equal); Writing – review & editing (equal). **Brett C. Johnson:** Conceptualization

© Author(s) 2024

(equal); Formal analysis (equal); Investigation (equal); Supervision (equal); Validation (equal); Visualization (lead); Writing – review & editing (equal).

DATA AVAILABILITY

The data that support the findings of this study are available from the corresponding author upon reasonable request.

REFERENCES

[1] J. M. Warrender, "Laser hyperdoping silicon for enhanced infrared optoelectronic properties," Appl. Phys. Rev. **3**, 031104 (2016).
[2] W. Yang, S. Q. Lim, and J. S. Williams, "Optical hyperdoping," in *Laser Annealing Processes in Semiconductor Technology* (Elsevier, 2021), pp. 323–356.
[3] S. Q. Lim and J. S. Williams, "Electrical and optical doping of silicon by pulsed-laser melting," in *Micro* (MDPI, 2021), Vol. 2, pp. 1–22.
[4] A. Luque, A. Martí, E. Antolín, and C. Tablero, "Intermediate bands versus levels in non-radiative recombination," Phys. B: Condens. Matter **382**, 320 (2006).
[5] W. Yang, A. J. Akey, L. A. Smillie, J. P. Mailoa, B. C. Johnson, J. C. McCallum, D. Macdonald, T. Buonassisi, M. J. Aziz, and J. S. Williams, "Au-rich filamentary behavior and associated subband gap optical absorption in hyperdoped Si," Phys. Rev. Mater. **1**, 074602 (2017).
[6] J. P. Mailoa *et al.*, "Room-temperature sub-band gap optoelectronic response of hyperdoped silicon," Nat. Commun. **5**, 3011 (2014).
[7] D. Recht *et al.*, "Supersaturating silicon with transition metals by ion implantation and pulsed laser melting," J. Appl. Phys. **114**, 124903 (2013).
[8] S. Q. Lim, A. Akey, E. Napolitani, P. Chow, J. Warrender, and J. Williams, "A critical evaluation of Ag-and Ti-hyperdoped Si for Si-based infrared light detection," J. Appl. Phys. **129**, 065701 (2021).
[9] S. Q. Lim, C. T.-K. Lew, P. Chow, J. Warrender, J. Williams, and B. Johnson, "Process-induced defects in Au-hyperdoped Si photodiodes," J. Appl. Phys. **126**, 224502 (2019).
[10] S. Q. Lim, C. T.-K. Lew, P. Chow, J. Warrender, J. Williams, and B. Johnson, "Toward understanding and optimizing Au-hyperdoped Si infrared photodetectors," APL Mater. **8**, 061109 (2020).
[11] S. S. Dissanayake, N. O. Pallat, P. K. Chow, S. Q. Lim, Y. Liu, Q. Yue, R. Fiutak, J. Mathews, J. S. Williams, J. M. Warrender, and M. J. Sher, "Carrier lifetimes in gold—hyperdoped silicon—influence of dopant incorporation methods and concentration profiles," APL Mater. **10**, 111106 (2022).
[12] Q. M. Hudspeth, M. Altwerger, P. K. Chow, M.-J. Sher, S. S. Dissanayake, W. Yang, J. Maurer, S. Q. Lim, J. S. Williams, H. Efsthadiadis, and J. M. Warrender, "Cellular breakdown and carrier lifetimes in gold-hyperdoped silicon," Semicond. Sci. Technol. **37**, 124003 (2022).
[13] J. M. Poate, *Laser Annealing of Semiconductors* (Elsevier, 2012).
[14] W. Yang, Q. Hudspeth, P. K. Chow, J. M. Warrender, N. Ferdous, E. Ertekin, G. Malladi, A. J. Akey, M. J. Aziz, and J. Williams, "Atomistic mechanisms for the thermal relaxation of Au-hyperdoped Si," Phys. Rev. Appl. **12**, 024015 (2019).
[15] H. Weman, A. Henry, T. Begum, B. Monemar, O. Awadelkarim, and J. Lindström, "Electrical and optical properties of gold-doped n-type silicon," J. Appl. Phys. **65**, 137 (1989).
[16] M. Valdinoci, L. Colalongo, A. Pellegrini, and M. Rudan, "Analysis of conductivity degradation in gold/platinum-doped silicon," IEEE Trans. Electron Devices **43**, 2269 (1996).
[17] A. Luque and A. Martí, "A metallic intermediate band high efficiency solar cell," Prog. Photovolt.: Res. Appl. **9**, 73 (2001).
[18] A. Luque, A. Martí, and C. Stanley, "Understanding intermediate-band solar cells," Nat. Photonics **6**, 146 (2012).
[19] N. Ferdous and E. Ertekin, "Atomic scale origins of sub-band gap optical absorption in gold-hyperdoped silicon," AIP Adv. **8**, 055014 (2018).
[20] D. Holmes, W. I. L. Lawrie, B. C. Johnson, A. Asadpoordarvish, J. C. McCallum, D. R. McCamey, and D. N. Jamieson, "Activation and electron spin resonance of near-surface implanted bismuth donors in silicon," Phys. Rev. Mater. **3**, 083403 (2019).
[21] L. Doolittle, "Rump: Rutherford backscattering spectroscopy analysis package," Nucl. Instrum. Methods Phys. Res., Sect. B **9**, 344 (1985).
[22] A. Hiraki, E. Lugujjo, and J. W. Mayer, "Formation of silicon oxide over gold layers on silicon substrates," J. Appl. Phys. **43**, 3643 (1972).
[23] G. Leclerc, L. Paquin, and F. Baratay, "Nonlinear silicon oxide growth patterns in a gold-silicon system," J. Mater. Res. **7**, 2458 (1992).
[24] J. Olea, G. González-Díaz, D. Pastor, I. Mártil, A. Martí, E. Antolín, and A. Luque, "Two-layer Hall effect model for intermediate band Ti-implanted silicon," J. Appl. Phys. **109**, 063718 (2011).
[25] J. Olea, G. González-Díaz, D. Pastor, E. García-Hemme, D. Caudevilla, S. Algaidy, F. Pérez-Zenteno, S. Duarte-Cano, R. García-Hernansanz, A. del Prado, and E. San Andrés, "Electronic transport properties of Ti-supersaturated Si processed by rapid thermal annealing or pulsed-laser melting," Semicond. Sci. Technol. **38**, 024001 (2022).
[26] A. Aldea, "Theory of the Hall effect in disordered systems: Impurity band conduction (II)," Phys. Status Solidi B **22**, 377 (1967).
[27] W. Yang, N. Ferdous, P. Simpson, J. Gaudet, Q. Hudspeth, P. Chow, J. Warrender, A. Akey, M. Aziz, E. Ertekin, and J. S. Williams, "Evidence for vacancy trapping in Au-hyperdoped Si following pulsed laser melting," APL Mater. **7**, 101124 (2019).
[28] S. M. Sze and K. K. Ng, *Physics of Semiconductor Devices*, 3rd ed. (John Wiley & Sons, 2007), Chap. 3.
[29] S. Brotherton, "Electrical properties of gold at the silicon-dielectric interface," J. Appl. Phys. **42**, 2085 (1971).
[30] In terms of the Ohmic contacts formed on our substrate control sample, we believe this is also a result of Si surface states pinning the Fermi level to 0.33 eV above the VB.[28]
[31] P. K. Chow, W. Yang, Q. Hudspeth, S. Q. Lim, J. S. Williams, and J. M. Warrender, "Observation of enhanced infrared absorption in silicon supersaturated with gold by pulsed laser melting of nanometer-thick gold films," J. Appl. Phys. **123**, 133101 (2018).

04 September 2024 02:21:17

© Author(s) 2024